



Universiteit
Leiden
The Netherlands

Core cross-linked polymeric micelles for specific iron delivery: inducing sterile inflammation in macrophages

Bauer, T.A.; Horvat, N.K.; Marques, O.; Chocarro, S.; Mertens, C.; Colucci, S.; ... ; Barz, M.

Citation

Bauer, T. A., Horvat, N. K., Marques, O., Chocarro, S., Mertens, C., Colucci, S., ... Barz, M. (2021). Core cross-linked polymeric micelles for specific iron delivery: inducing sterile inflammation in macrophages. *Advanced Healthcare Materials*, 10(19).
doi:10.1002/adhm.202100385

Version: Publisher's Version

License: [Creative Commons CC BY-NC 4.0 license](https://creativecommons.org/licenses/by-nc/4.0/)

Downloaded from: <https://hdl.handle.net/1887/3216831>

Note: To cite this publication please use the final published version (if applicable).

Core Cross-Linked Polymeric Micelles for Specific Iron Delivery: Inducing Sterile Inflammation in Macrophages

Tobias A. Bauer, Natalie K. Horvat, Oriana Marques, Sara Chocarro, Christina Mertens, Silvia Colucci, Sascha Schmitt, Luca M. Carrella, Svenja Morsbach, Kaloian Koynov, Federico Fenaroli, Peter Blümmler, Michaela Jung, Rocio Sotillo, Matthias W. Hentze,* Martina U. Muckenthaler,* and Matthias Barz*

Iron is an essential co-factor for cellular processes. In the immune system, it can activate macrophages and represents a potential therapeutic for various diseases. To specifically deliver iron to macrophages, iron oxide nanoparticles are embedded in polymeric micelles of reactive polysarcosine-*block*-poly(*S*-ethylsulfonyle-L-cysteine). Upon surface functionalization via dihydrolipoic acid, iron oxide cores act as crosslinker themselves and undergo chemoselective disulfide bond formation with the surrounding poly(*S*-ethylsulfonyle-L-cysteine) block, yielding glutathione-responsive core cross-linked polymeric micelles (CCPMs). When applied to primary murine and human macrophages, these nanoparticles display preferential uptake, sustained intracellular iron release, and induce a strong inflammatory response. This response is also demonstrated *in vivo* when nanoparticles are intratracheally administered to wild-type C57Bl/6N mice. Most importantly, the controlled release concept to deliver iron oxide in redox-responsive CCPMs induces significantly stronger macrophage activation than any other iron source at identical iron levels (e.g., Feraheme), directing to a new class of immune therapeutics.


1. Introduction

Diseases, such as cancer, atherosclerosis, traumatic nerve injury, and autoimmune disorders are hallmarked by inflammation, whereby infiltration of innate immune cells can exacerbate the disease condition.^[1–5] Phagocytic cells, such as monocytes and monocyte-derived macrophages comprise a significant proportion of these infiltrating cells, and a growing number of macrophage subtypes were identified, which are characterized by different functional capabilities, depending on niche-derived stimuli, such as cytokines, chemokines, and metabolites.^[6–10] Recruited monocyte-derived macrophages residing in the periphery of solid tumors can mediate adaptive immunity, promote angiogenesis, tissue remodeling and repair, and often contribute to the aggressiveness of a cancer's invasive front.^[11–13] Apart from

T. A. Bauer, Prof. M. Barz
Leiden Academic Centre for Drug Research (LACDR)
Leiden University
Einsteinweg 55, Leiden 2333CC, The Netherlands
E-mail: m.barz@lacdr.leidenuniv.nl

T. A. Bauer, Dr. L. M. Carrella, Prof. M. Barz
Department of Chemistry
Johannes Gutenberg University Mainz
Duesbergweg 10-14, Mainz 55128, Germany

N. K. Horvat, Prof. M. W. Hentze
European Molecular Biology Laboratory (EMBL)
Collaboration for Joint PhD Degree between EMBL and the Faculty of Biosciences
University of Heidelberg
Meyerhofstr. 1, Heidelberg 69117, Germany
E-mail: hentze@embl.org

 The ORCID identification number(s) for the author(s) of this article can be found under <https://doi.org/10.1002/adhm.202100385>

© 2021 The Authors. Advanced Healthcare Materials published by Wiley-VCH GmbH. This is an open access article under the terms of the Creative Commons Attribution-NonCommercial License, which permits use, distribution and reproduction in any medium, provided the original work is properly cited and is not used for commercial purposes.

DOI: 10.1002/adhm.202100385

N. K. Horvat, Dr. O. Marques, Dr. C. Mertens, S. Colucci,
Prof. M. U. Muckenthaler
Molecular Medicine Partnership Unit (MMPU)
Otto-Meyerhof-Zentrum
Im Neuenheimer Feld 350, Heidelberg 69120, Germany
E-mail: martina.muckenthaler@med.uni-heidelberg.de

N. K. Horvat, Prof. R. Sotillo, Prof. M. U. Muckenthaler
Translational Lung Research Center Heidelberg (TLRC)
German Center for Lung Research (DZL)
University of Heidelberg
Im Neuenheimer Feld 350, Heidelberg 69120, Germany

Dr. O. Marques, Dr. C. Mertens, S. Colucci, Prof. M. U. Muckenthaler
Department of Pediatric Oncology, Hematology, Immunology, and Pulmonology
Heidelberg University Hospital
Im Neuenheimer Feld 350, Heidelberg 69120, Germany

S. Chocarro, Prof. R. Sotillo
Department of Molecular Thoracic Oncology
German Cancer Research Center (DKFZ)
Im Neuenheimer Feld 280, Heidelberg 69120, Germany

S. Schmitt, Dr. S. Morsbach, Dr. K. Koynov
Max Planck Institute for Polymer Research
Ackermannweg 10, Mainz 55128, Germany

immune functions, macrophages play a pivotal role in maintaining iron homeostasis, as they recycle hemoglobin-derived iron from senescent red blood cells.^[14–17] The intricate connection between the immune function of macrophages and their role in iron metabolism was demonstrated by the exposure to metabolites, such as free heme or iron, that directly affect the macrophage activation state, leading to not only changes in the expression of iron-regulatory genes but also in innate immune effector functions.^[1,18] By locally applying iron in the form of superparamagnetic iron oxide nanoparticles (SPIONs) within the tumor microenvironment (TME), macrophages become activated, a process that can correlate with inhibition of tumor growth.^[1,19] In previous studies, ferumoxytol (Feraheme, Riensol), a formulation of an iron oxide nanoparticle in a matrix of covalently cross-linked carbohydrates (polyglucose sorbitol carboxymethylether), was used as iron source.^[19–23] Despite its approval for the treatment of iron deficiency anemia in patients with chronic kidney disease, the original intention of ferumoxytol was as a contrast agent for magnetic resonance imaging designed for minimal iron release.^[24–30] We now propose that delivery systems which allow for controlled iron release in the TME can serve as immunotherapeutic agent.

SPION-loaded core cross-linked polymeric micelles (SPION-CCPMs) were developed based on polysarcosine-block-poly(*S*-ethylsulfonylethyl-L-cysteine) (pSar-*b*-pCys(SO₂Et)) copolypept(o)ides.^[31,32] In these systems, cross-linking by chemoselective disulfide formation features glutathione (GSH)-dependent particle degradation inside the endo- or phagosomal pathway of macrophages.^[33]

2. Results and Discussion

The polymer synthesis was performed by nucleophilic ring-opening polymerization of α -amino acid *N*-carboxyanhydrides (NCAs), yielding polypept(o)ides of pSar-*b*-pCys(SO₂Et).^[31,32,34] As shown in **Figure 1**, block copolymers were obtained using a bifunctional initiator approach, leading to polymers P1–P3 with chain lengths of 170 to 225 for polysarcosine and 17 to 31 for poly(*S*-ethylsulfonylethyl-L-cysteine), well suited for steric shielding and cross-linking.^[35,36] The syntheses were accomplished on a gram-scale, yielding 2.9 g of P2 and 2.3 g of P3 (Scheme S1, Table S1, and Figures S1–S5, Supporting Information) demonstrating the scalability of the presented approach. For nanoparticle preparation, oleic acid-coated SPIONs (γ -maghemite, Fe₂O₃, $D =$

6 nm) were solubilized with the amphiphilic pSar-*b*-pCys(SO₂Et) block copolymers, cross-linked with dihydrolipoic acid, and labeled on the amine end-group with Cy5-NHS ester (Figure 1). During co-self-assembly, initial solvent mixtures of chloroform and dimethyl sulfoxide (DMSO) were exchanged stepwise to pure DMSO and water, resulting in SPION-CCPMs as an aqueous dispersion. In addition to disulfide bond formation, dihydrolipoic acid enables direct grafting onto the iron oxide nanoparticle surface by substituting oleic acid, connecting the respective building blocks and stabilizing SPION encapsulation (Figure 1D). Unconjugated dye, residual oleic acid, and free polymer were removed by extraction and repetitive ultra-filtration (MWCO 100 kDa) yielding SPION-CCPM^{Cy5} as a dark green aqueous dispersion (Figure 1E; Figure S9, Supporting Information). To serve as control nanoparticles, empty CCPMs were prepared from pSar-*b*-pCys(SO₂Et), according to previous reports (Table S2, Figures S6, S7, Supporting Information).^[35,37]

The illustration of SPION-CCPMs as spherical structures containing multiple SPION cores was derived from nanoparticle characterization, which is summarized in Figure 1 and **Table 1**. According to single-angle dynamic light scattering (DLS), co-self-assembly of oleic acid-coated SPIONs and P3 (mass ratio 1:1) yielded micelles with a hydrodynamic diameter (D_h) of 71 nm (Figure 1A), whereby the size slightly increased to $D_h = 82$ nm upon cross-linking, dye conjugation, and particle purification. Importantly, the narrow size distribution ($PDI \leq 0.16$) of SPION-CCPMs^{Cy5} remained identical when particles were lyophilized and re-constituted in water (SPION-CCPM^{Cy5}-Lyo), which facilitates their scalability and pharmaceutical use.^[38]

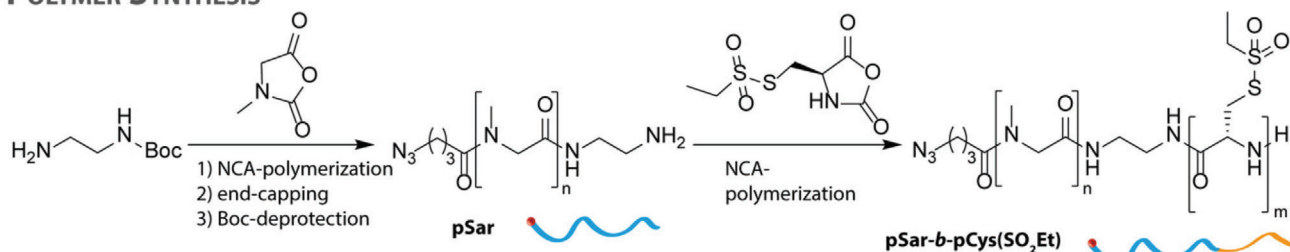
Morphological analysis of SPION-CCPMs by atomic force microscopy (AFM) revealed spherical structures with sizes below 100 nm (Figure 1C), congruent with DLS and fluorescence correlation spectroscopy (FCS) (Table 1; Figure S10, Supporting Information). Transmission electron microscopy (TEM) was used to elucidate the encapsulated SPION cores. SPIONs were organized in patterns of local clusters with total dimensions below 50 nm containing multiple cores each (Figure 1C; Figure S11, Supporting Information). The individual SPION cores showed diameters of 6 to 10 nm. In contrast, oleic acid-coated SPIONs were randomly arranged (Figure S12, Supporting Information). Since the polymer shell could not be visualized due to large contrast discrepancies, the observed local clustering emphasizes successful encapsulation of iron oxide nanoparticles into CCPMs.^[39–41] Taken together, AFM and TEM analysis affirm the structure of SPION-CCPMs as spherical nano-sized containers with multiple iron oxide nanoparticles embedded. The quantification of iron in lyophilized SPION-CCPMs was performed by thermogravimetric analysis (TGA) in a pure O₂ atmosphere. At these conditions, the polymeric matrix is entirely oxidized, and the remnant corresponds to iron oxide (Fe₂O₃) (Figure 1B).^[42] For SPION-CCPMs, an iron oxide content of 33 weight% was determined (Table 1). Moreover, SPION-CCPMs were analyzed by Fourier transform infrared (FT-IR) spectroscopy. Characteristic peaks at 2853, 1738, and 1709 cm⁻¹ corresponding to oleic acid dissipated upon encapsulation, and peaks of the polymer backbone (3470 cm⁻¹, 3275 cm⁻¹ (amide N–H), 1633 cm⁻¹ (amide C=O)) were detected (Figure S8, Supporting Information), indicating complete replacement of the oleic acid-coating and successful surface functionalization by lipoic acid.^[43]

Dr. F. Fenaroli
Department for Biosciences
University of Oslo
Blindernveien 31, Oslo 0371, Norway

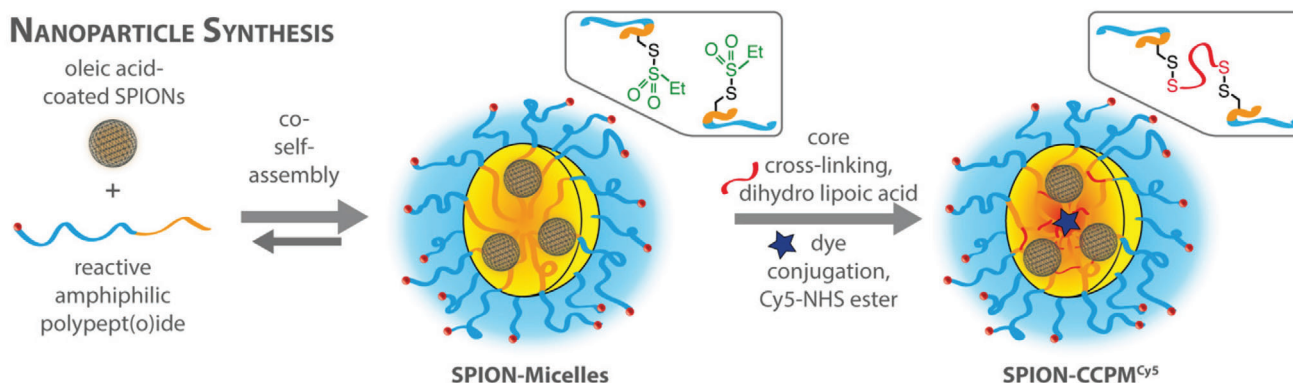
Dr. P. Blümmler
Institute of Physics
Johannes Gutenberg University Mainz
Staudingerweg 9, Mainz 55128, Germany

Dr. M. Jung
Institute of Biochemistry I
Faculty of Medicine
Goethe-University Frankfurt
Theodor-Stern-Kai 7, Frankfurt am Main 60590, Germany

POLYMER SYNTHESIS



NANOPARTICLE SYNTHESIS



NANOPARTICLE CHARACTERIZATION

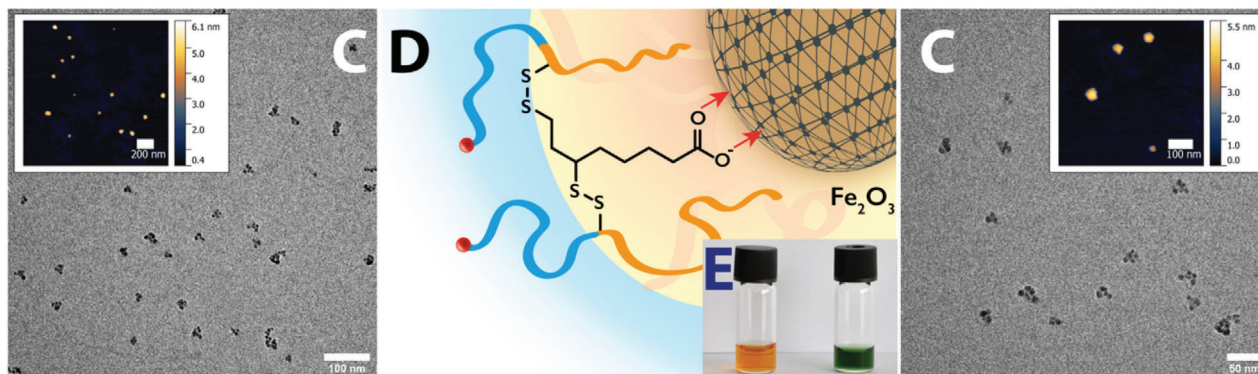
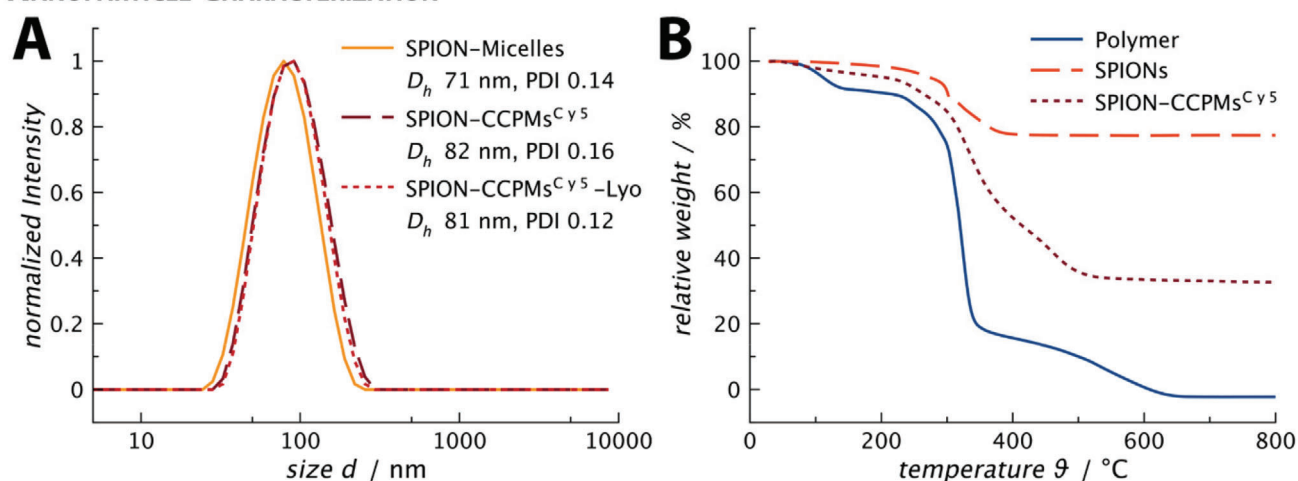


Figure 1. Polymer and nanoparticle synthesis, and characterization of SPION-CCPMs. A) Single-angle DLS of SPION-Micelles and SPION-CCPMs^{Cy5} before and after lyophilization and redispersion in water (lyo). B) Iron oxide quantification by TGA in pure O₂ atmosphere. C) Analysis of SPION-CCPMs^{Cy5} by AFM and TEM. D) Illustrated surface grafting by the carboxyl group of the lipoic acid cross-linker in the micellar core. E) Image of SPION-CCPM dispersions in MilliQ water before (left) and after dye-labeling (right).

Table 1. Summary of the nanoparticle characterization.

Particle	Polymer ^{a)}	wt% Fe ₂ O ₃ ^{b)} [%]	D _h ^{c)} [nm]	D _h ^{d)} [nm]	ξ-potential ^{c)} [mV]
SPION-CCPM ^{Cy5}	P3, pSar ₁₇₀ -b-pCys(SO ₂ Et) ₂₇	33.0	82	72	-5.1
CCPM ^{Cy5}	P1, pSar ₂₂₅ -b-pCys(SO ₂ Et) ₃₁	–	49	47	-4.2

^{a)} pSar chain lengths relative to pSar standards, pCys(SO₂Et) chain lengths derived from ¹H NMR ^{b)} TGA in pure O₂ atmosphere ^{c)} Single angle DLS at a scattering angle of 173° ^{d)} fluorescence correlation spectroscopy.

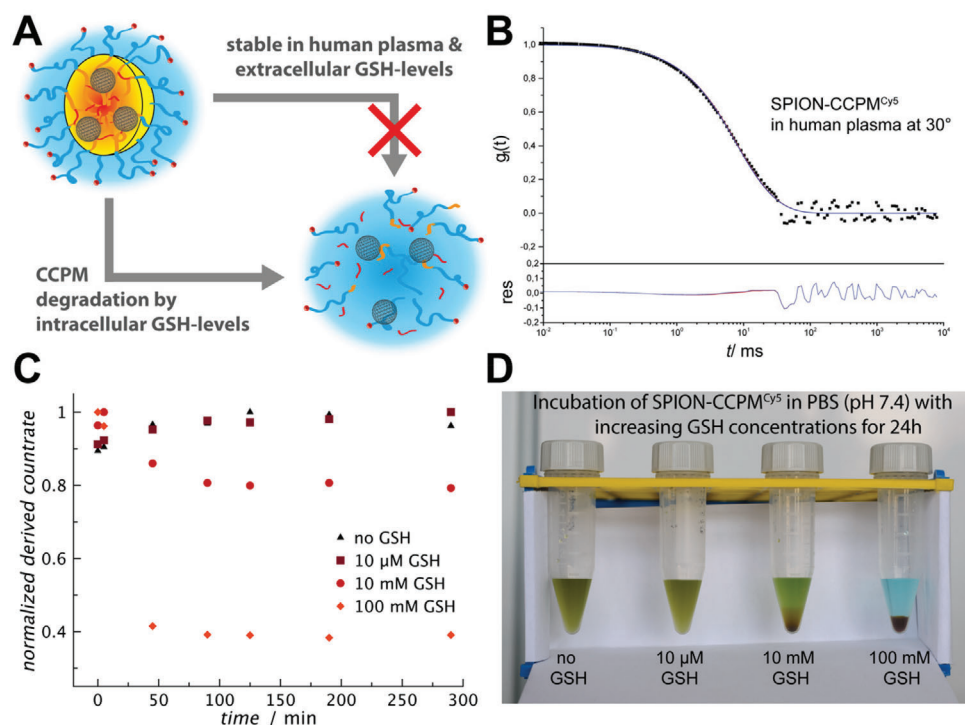


Figure 2. SPION-CCPMs display colloidal stability and stimuli-responsive degradation. A) Concept of intracellular iron release inside macrophages B) Multi-angle DLS of SPION-CCPM^{Cy5} in undiluted human plasma: autocorrelation function $g_1(t)$ for an exemplary scattering angle of 30° together with fits with (blue line) and without (red line) additional aggregate term (upper graph), and the corresponding residuals between fit w/o aggregate and correlation function. C) Glutathione (GSH)-induced particle degradation after incubation in carbonate buffer (pH 7.4) at 37 °C detected by single-angle DLS. D) GSH-induced degradation performed in phosphate buffer (pH 7.4, 37 °C) after 24 h.

The superparamagnetic nature of SPION-CCPMs was confirmed by magnetization hysteresis loops recorded at temperatures of 300 and 5 K. No significant remanence magnetization could be detected and a blocking temperature of 42 K was obtained corresponding to iron oxide nanoparticles with a diameter of ≈ 10 nm (Figure S13, Supporting Information).^[44] Accordingly, the SPION-CCPM^{Cy5} dispersion showed response to magnetic fields (Figure S14, Supporting Information) without aggregation. In an in vitro setting, particles could be guided by a combined dipolar/quadrupolar magnetic field (Video S1, Supporting Information).^[45,46] However, no signs of magnetic guidance were distinguishable in zebrafish larvae (see Supporting Information for further details).

To account for colloidal stability, SPION-CCPMs were analyzed by multi-angle DLS in human blood plasma, following the procedure by Rausch et al.^[47] Here, no aggregation was detected after incubation of SPION-CCPM^{Cy5} in human blood plasma at a nanoparticle concentration of 0.1 g·L⁻¹ (Figure 2B).

Moreover, SPION-CCPM^{Cy5} remained intact even during analysis by gel permeation chromatography (GPC) in hexafluoroisopropanol (Figure S8, Supporting Information), a good solvent for pSar-b-pCys(SO₂Et) copolymers. The absence of unconjugated dye was further verified by FCS (Figure S10, Supporting Information).^[48] SPION-CCPM^{Cy5} exhibit a slightly negative ζ -potential of -5.1 mV, comparable to empty CCPMs, accounting for efficient compensation of the iron oxide surface charge by lipoic acid as well as sufficient shielding by the polysarcosine corona (Figure S8, Supporting Information).^[49] The stimuli-responsive behavior of disulfide cross-linked SPION-CCPMs was evaluated by DLS in carbonate buffer (pH 7.4) at GSH concentrations present in the endo-phagosomal compartments of macrophages.^[50] At extracellular GSH levels (10 μ M) the derived count rate remains constant, while a decrease was observed at intracellular GSH levels (10 mM) indicating particle degradation (Figure 2C).^[35] Interestingly, when conducted in phosphate buffer (pH 7.4), precipitation of iron oxide/phosphate is observed

for SPION-CCPMs treated with GSH concentrations above $10\ \mu\text{M}$ (Figure 2D), exemplifying the combination of stability in blood-like conditions with triggered (redox-dependent) release of the encapsulated iron.

When tested in cell lines or primary murine and human cells, the internalization of nanoparticles was measured by intracellular fluorescent intensity using fluorescence-activated cell sorting (FACS) and fluorescence microscopy. In a co-culture of Lewis lung carcinoma cells (LLCs) and primary murine bone marrow-derived macrophages (BMDMs), SPION-CCPMs appear to sequester mainly in macrophages. Vice versa, LLCs accumulate more CCPMs than SPION-CCPMs (Figure 3A), suggesting that iron released from SPION-CCPMs may further reduce SPION-CCPM uptake in LLCs, in a negative feedback manner. The iron released from SPION-CCPMs likely stimulates BMDMs' uptake rate. This leads to a remarkable ≈ 100 -fold difference in relative nanoparticle uptake between the epithelial and myeloid cell type. These results indicate that SPION-CCPMs are preferably taken up by macrophages and not by other cell types (primary hepatocytes, LLCs; Figure S17, Supporting Information). To further explore whether SPION-CCPMs release iron inside macrophages and if it is metabolically active, we analyzed the expression of iron regulatory genes in BMDMs. After 1 h incubation, SPION-CCPMs were detected in BMDMs (Figure S18, Supporting Information) but iron was not detected to the same extent as BMDMs treated with a dose-matched iron source ferric ammonium citrate (FAC) (Figure 3B). After 24 h, BMDMs treated SPION-CCPMs show iron accumulation to a similar extent as FAC treated BMDMs (Figure 3B), indicating a sustained release profile.

At the molecular level, iron accumulation decreased transferrin receptor 1 mRNA (*Tfrc*) and protein expression (TFR1) (Figure 3C) also seen in BMDMs treated with FAC ($20\ \mu\text{M}$) or lipopolysaccharide (LPS), which can trigger iron sequestration in pro-inflammatory macrophages.^[7,11,15]

Iron accumulation in cells triggers oxidative stress and target gene expression of the oxidative stress responsive transcription factor nuclear factor E2-related factor-2(Nrf2)/BTB and CNC homolog 1 basic leucine zipper (bZIP) transcription factor 1 (Bach1) signaling pathway.^[51] Expression of two Nrf2 target genes, *HO-1* (Figure 3C) and *Fpn1* (Figure 3D), are strongly induced in macrophages treated with SPION-CCPMs. At an early time point (4 h), ROS levels induced by SPION-CCPM treatment were high in the cytoplasm and low in nuclear and mitochondrial regions (Figure 3E), suggesting that iron is released into the cytoplasm soon after nanoparticle internalization. Of note, 18 h after SPION-CCPM treatment, ROS detection shifted to nuclear and mitochondrial compartments (Figure 3F), similar to FAC treated cells. Importantly, CCPMs did not increase ROS levels in BMDMs, suggesting that iron released from the SPION-CCPMs specifically triggers ROS production. Taken together, these data support the concept of SPION-CCPMs, which degrade slowly so that BMDMs safely handle internalized particles without detectable cellular toxicity (Figure S19, Supporting Information). Most importantly, the released iron is metabolically active and able to alter iron metabolism and oxidative defense.

The exposure of macrophages to heme or non-transferrin bound iron has been reported to activate an inflammatory state, hallmarked by increased expression of inflammatory cytokines,

such as interleukin (IL)- $1\alpha/\beta$, IL-6, and tumor necrosis factor (TNF) α , as well as elevated surface proteins, such as cluster of differentiation (CD) 86, CD80, and Class II major histocompatibility complex molecules (MHC II).^[1,19,52] We analyzed these important markers of inflammation in BMDMs exposed to LPS or IL4, serving as positive and negative controls, respectively, and $20\ \mu\text{M}$ of FAC, SPION-CCPMs, as well as the non-loaded CCPMs. BMDMs treated with SPION-CCPMs remarkably increase the expression of MHC II, CD80, CD301, and CD86, similar to LPS stimulated cells (Figure 4A). Similarly, inflammatory cytokines and enzymes, such as *Tnfa*, *Il6*, *Il1b*, *Nos2*, and *Cxcl10* were significantly upregulated (Figure 4B). In contrast, expression of the mannose receptor, CD206, an indicator of anti-inflammatory activation, was reduced in BMDMs exposed to SPION-CCPMs compared to those with CCPMs (Figure 4A). Notably, the specific inflammatory response to SPION-CCPMs was also reflected in human macrophages (Figure 4D; Figure S20, Supporting Information).

Iron delivery by SPION-CCPMs induces a remarkably robust pro-inflammatory response in human and murine macrophages (Figure 4), an effect that is significantly more pronounced than for Feraheme (ferumoxytol) at identical iron levels. To understand the basis of this effect, we tested individual components of the polypept(o)ide-based delivery system, such as L-cysteine, S-ethylsulfonyl-L-cysteine (L-Cys(SO₂Et)) or analogous S-ethylsulfonyl-L-homocysteine (L-Hcy(SO₂Et), either alone or in combination with heme and FAC. When added with iron, L-Cys(SO₂Et) and L-Hcy(SO₂Et) induced expression of MHC II and CD86, albeit to a much lower extent than intact SPION-CCPMs (Figure 4E; Figure S21, Supporting Information). We thus propose that the chemical nature of the nanoparticles together with the intracellular iron release are responsible for the observed strong inflammatory responses. Examination of the gene expression changes (Figure 4) indicate sterile inflammation is triggered by SPION-CCPMs, resembling LPS-like inflammation in macrophages. Differences were observed for mRNA expression of arginase-1, Nrf2 target genes, NAD(P)H dehydrogenase (quinone) 1, and Glutathione S-Transferase Mu 1 (Figure S22, Supporting Information). We thus speculate that SPION-CCPM treatment induces a combination of signaling pathways through both iron and inflammatory patterns.^[22]

To verify that SPION-CCPMs can also induce inflammation *in vivo*, the nanoparticles were applied to wild-type C57Bl/6N mice (Figure 5A). Female mice, aged 6–8 weeks, were intratracheally instilled with phosphate-buffered saline (PBS) or SPION-CCPMs. At 4 and 24 h post-treatment, mice were sacrificed and evaluated for immune cell recruitment and iron content in the lungs. Among other indications, we expect the developed SPION-CCPMs to be highly beneficial for the application as an adjuvant in cancer therapy.^[1,53] Since the lungs are densely populated with macrophages and offer the advantage to apply SPION-CCPMs non-invasively to macrophages reducing off-target immune activation in other organs, intratracheal administration is a preferable application route.^[12,54–57]

We found that at 24 h after instillation, non-heme iron content increased approximately threefold in the lungs of SPION-CCPMs administered mice compared to PBS administered mice (Figure 5B). Furthermore, FACS analysis demonstrated that SPION-CCPMs could be detected in both, alveolar (AM) and

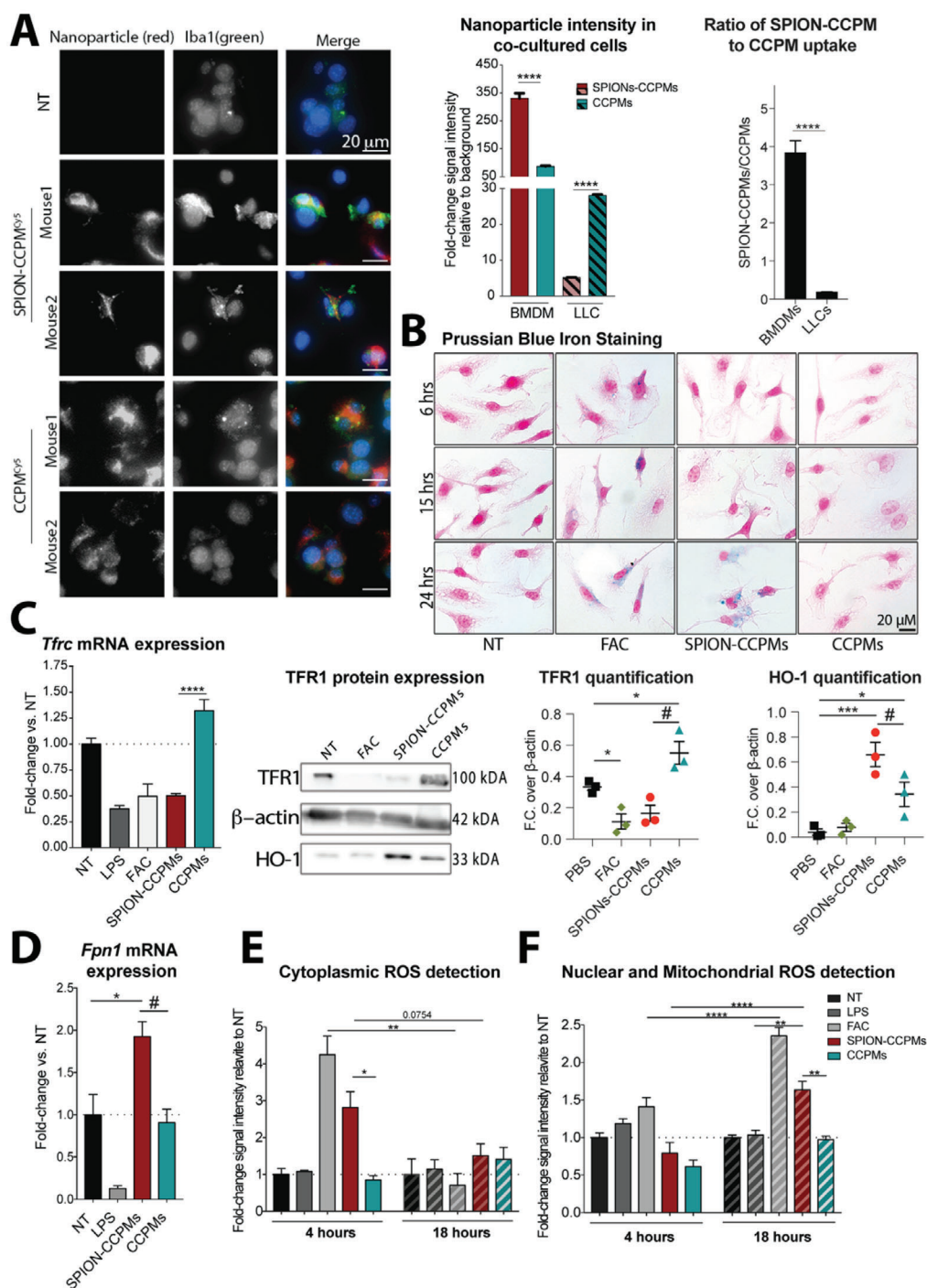


Figure 3. In vitro analysis of SPION-CCPMs. A) Co-culture of LLCs and BMDMs incubated with SPION-CCPMs^{Cy5} and CCPMs^{Cy5} or not treated (NT). Representative fluorescence microscopy images and Cy5 fluorescence detection by FACS after 24 h. B) Detection of released iron by Perls' Prussian blue staining. Cells were counterstained with nuclear fast red (pink). C) Detection of transferrin receptor (*Tfr*) mRNA as well as TFR1 and heme oxygenase 1 (*HO-1*) protein by qPCR and western blot. mRNA expression was corrected to *Rpl19* expression. D) Ferroportin (*Fpn1*) mRNA expression after 6 h. E) Cytoplasmic or F) nuclear and mitochondrial ROS detection using CELLROX Orange and CELLROX Green probes in BMDMs after 4- and 18-h. Fluorescent intensities produced by ROS probes were measured by FACS and represented as fold-change compared to non-treated (NT) condition. Data reported as $n \pm$ standard error of the mean (SEM) and representative of three independent experiments. One-way ANOVA(*) or Student's *t*-test(#) : * $p < 0.01$, ** $p < 0.001$, and *** $p < 0.0001$.

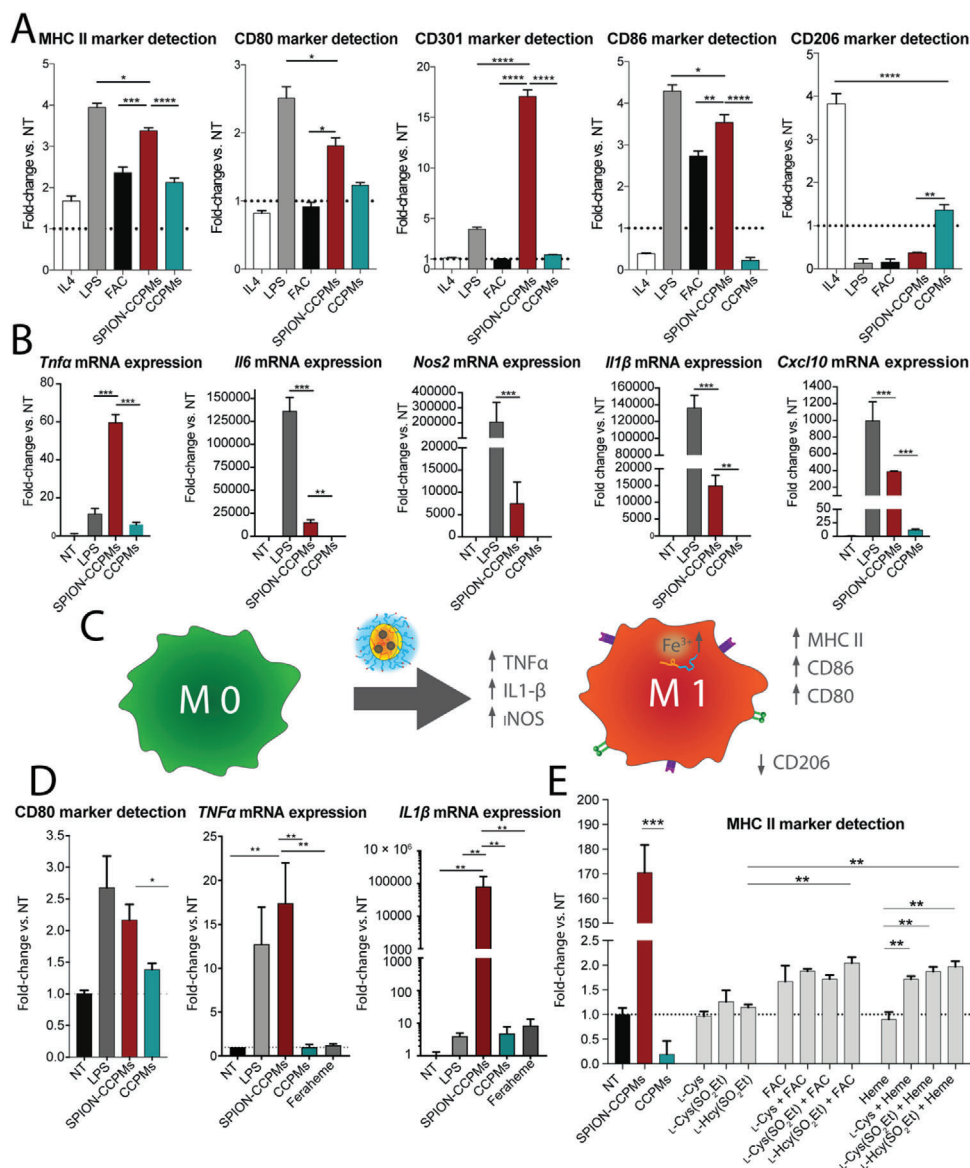


Figure 4. SPION-CCPMs induce sterile inflammation in macrophages. A) Cell surface protein expression and B) mRNA expression levels of inflammatory cytokines and chemokines in primary murine BMDM after 24 or 6 h, respectively. C) Illustration of the inflammatory response. D) Upregulation of inflammatory mRNA and protein expression in human macrophages. E) Cell surface marker MHC II expression for individual CCPM components. All graphs in (A-E) represent data as fold change compared to the non-treated condition (NT) and mRNA expression were corrected to *Rpl19*. Data reported as $n \pm$ SEM and representative of three independent experiments. One-way ANOVA: * $p < 0.05$, ** $p < 0.01$, *** $p < 0.001$, and **** $p < 0.0001$.

interstitial (IM) macrophages as early as 4 h following application. The intensity of SPION-CCPMs increased significantly in both cell types at the 24 h time point (Figure 5C), indicating that IM and AM are rapidly taking up SPION-CCPMs. We speculate that the difference in uptake between these two populations may be explained by their residing location within the lungs. The intratracheal instillation applied here delivers SPION-CCPMs to the bronchus of the lungs where IMs are mainly localized. This may explain the brighter SPION signal in IMs 4 h after SPION-CCPMs application compared to AM that are located in the alveolar space and thus take longer time to reach.^[58,59] We next evaluated the inflammatory response in the lungs of mice upon administration of either PBS or SPION-CCPMs. Cell surface

marker expression in AM and IM were quantified by FACS, and mRNA expression of pro-inflammatory cytokines and enzymes were analyzed in total lung tissue. At both time points analyzed, AM showed increased expression of CD80 (a known inflammatory protein) and lacked expression of C-Mer proto-oncogene tyrosine kinase (MerTK), a protein expressed under conditions when inflammation resolves, demonstrating macrophage inflammatory activation by SPION-CCPM administration.^[13,60] IM were also responsive to SPION-CCPMs, showing reduced CD71 levels at the 24 h time point indicating a time-dependent intracellular degradation of SPION-CCPMs triggering a well-known response to iron accumulation (Figure 5D). This observation parallels our findings of SPION-CCPM treatment of BMDMs in cell

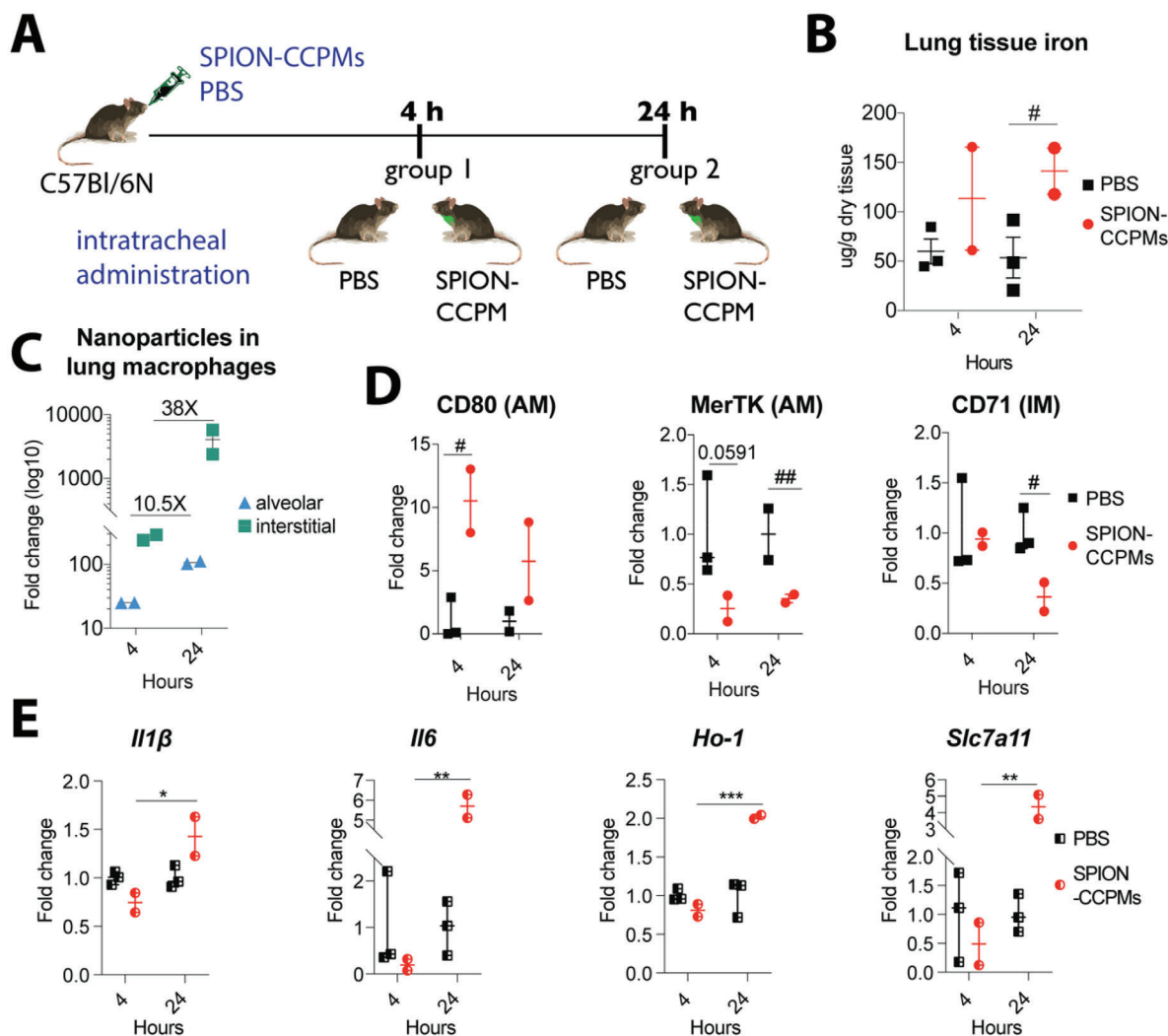


Figure 5. SPION-CCPMs induce inflammation in vivo. A) C57Bl/6 mice were analyzed 4 and 24 h after intratracheal administration of SPION-CCPMs or PBS as control. B) non-heme iron levels in lung tissue. C) Nanoparticle uptake in interstitial (IM) and alveolar (AM) macrophages. D) Cell surface protein expression on AM and IM. E) Analysis of mRNA expression of inflammatory cytokines and enzymes in total lung tissue. One-way ANOVA (*) or Student's *t*-test (#): * $p < 0.05$, ** $p < 0.01$, *** $p < 0.001$, and **** $p < 0.0001$.

culture (Figure 3B,C). The inflammatory response in lung tissue was further substantiated by showing time-dependent expression of the pro-inflammatory cytokines *Il1β* and *Il6*, as well as of oxidative stress response enzymes *Ho-1* and *Slc7a11* (Figure 5E). Notably, the delayed inflammatory response program at the 24 h time point substantiates findings in cultured cells (Figure 4) that suggest that SPION-CCPMs induce inflammation distinctly from LPS.^[61] Taken together, we show that SPION-CCPMs induce sterile activation of macrophages in cell-based assays and in the mouse lung, illustrating the significant potential for the activation of macrophages as an adjuvant therapy.

3. Conclusion

Our study demonstrates that specific delivery of an iron source to macrophages can trigger pronounced pro-inflammatory responses, both in vitro (primary murine and human cells)

and in vivo (C57Bl/6N mouse model). The design concept of polypept(o)ide-based SPION-CCPMs combines steric shielding and surface functionalization of SPIONs featuring colloidal stability and stimuli-responsive degradation, whereby the iron becomes available to macrophages upon internalization within 24 h by cleavage of the disulfide cross-links in the nanoparticle core. In primary murine and human macrophages, the sustained release of iron induces sterile inflammation as indicated by pro-inflammatory surface marker expression and cytokine secretion, resembling a shift toward an M1-like phenotype. This effect was confirmed in vivo following intratracheal administration of SPION-CCPMs to wild-type C57Bl/6N mice. Due to the immunomodulatory properties, SPION-CCPMs outcompete established iron oxide nanoparticles like Feraheme, making them a promising adjuvant therapy for the treatment of diseases, such as in autoimmune disorders, traumatic nerve injury, or interventions of the TME of solid cancers.

4. Experimental Section

Materials and Instrumentation: Unless stated otherwise, solvents were purchased from Sigma Aldrich. THF and n-hexane were dried over Na and freshly distilled prior to use. DMF was bought from Acros (99.8%, Extra Dry over Molecular Sieve), freshly freeze-pumped prior to use to remove residual dimethyl amine, and handled in the absence of light. HFIP was purchased from Fluorochem, deuterated solvents from Deutero, and were used as received. MilliQ water was prepared using a MILLI-Q Reference A+ System. Water was used at a resistivity of $18.2 \text{ M}\Omega\text{-cm}^{-1}$ and total organic carbon of <5 ppm. Diphosgene was purchased from Alfa Aesar. Sarcosine was bought from Sigma Aldrich and dried in vacuum before NCA synthesis. *N-tert*-butoxycarbonyl (Boc)-1,2-diaminoethane and *N,N*-diisopropyl ethylamine (DIPEA) were purchased from Sigma Aldrich, fractionally distilled and stored at -78 and -20 °C, respectively. Oleic acid coated iron oxide nanoparticles were obtained from Sanofi-Aventis Deutschland GmbH, as well as obtained from Ocean Nanotech. D,L-Lipoic acid was bought from TCI Europe. Pentafluorophenyl trifluoroacetate, tris(2-carboxyethyl)phosphine (TCEP-HCl) and acetic acid anhydride were obtained from Sigma Aldrich and used without further purification. Cyanine 5 NHS Ester was obtained from Lumiprobe GmbH. Human blood plasma for DLS measurements was collected at the Transfusion Center of the University Clinic of Mainz (Germany) from ten healthy donors after physical examination and after obtaining informed consent in accordance with the Declaration of Helsinki. The study was approved by the local ethics committee "Landesärztekammer Rheinland-Pfalz" (837.439.12 (8540-F)). All plasma batches were pooled and stored at -20 °C.

Nuclear Magnetic Resonance: ^1H , ^{19}F , and ^{13}C NMR spectra were recorded on a Bruker Avance II 400 at room temperature at a frequency of 400, 376, and 101 MHz and on a Bruker Avance III HD 300 at room temperature at a frequency of 300, 282, and 75 MHz. DOSY spectra were recorded on a Bruker Avance III HD 400 (400 MHz). Calibration of the spectra was achieved using the solvent signals. NMR spectra were analyzed with MestReNova version 12.0.4 from Mestrelab Research S.L. Degrees of polymerization (X_n) were calculated by comparing the integral of the initiator peak and the integrals of the protons for pSar and pCys(SO_2Et).

Infrared and UV-Vis Spectroscopy: Attenuated total reflectance FT-IR spectroscopy was performed on a FT/IR-4100 (Jasco) with an ATR sampling accessory (MIRacle, Pike Technologies). IR spectra were analyzed using Spectra Manager 2.0 (Jasco) for integration. NCA polymerization was monitored by FT-IR spectroscopy. UV-vis spectra were recorded using a Jasco V-630 spectrophotometer (1 cm \times 1 cm quartz cell).

Gel Permeation Chromatography: Analytical GPC was performed using HFIP as eluent, which contained $3 \text{ g}\cdot\text{L}^{-1}$ of potassium trifluoroacetate at a flow rate of $0.8 \text{ mL}\cdot\text{min}^{-1}$ at 40 °C. GPC columns were packed with modified silica (PFG-columns, particle size $7 \mu\text{m}$, porosity 100 \AA , and 1000 \AA) purchased from Polymer Standards Service GmbH. Poly(methyl methacrylate) standards (Polymer Standards Service GmbH) and pSar standards were used for calibration and toluene was used as the internal standard.^[62] A refractive index detector (G1362A RID, JASCO) and a UV detector ($\lambda = 230 \text{ nm}$, UV-2075+, JASCO) were used for polymer detection and analysis was performed using PSS WinGPC from PSS Polymer Standards Service GmbH.

Dynamic Light Scattering: Single-angle DLS measurements were performed with a ZetaSizer Nano ZS instrument (Malvern Instruments Ltd., Worcestershire, UK) equipped with a He-Ne laser ($\lambda = 632.8 \text{ nm}$) as the incident beam. All measurements were performed at 25 °C and a detection angle of 173° unless stated otherwise. Disposable polystyrene cuvettes (VWR, Darmstadt, Germany) were used for single-angle DLS measurements. Disposable folded capillary cells (Malvern Instruments Ltd., Worcestershire, UK) were employed for zeta potential measurements. Zeta potential measurements were conducted in solutions containing 3 mM sodium chloride. Cumulant size, polydispersity index (PDI), and size distribution (intensity weighted) histograms were calculated based on the autocorrelation function of the samples, with automated position and attenuator adjustment at multiple

scans. The derived count rate was used for aggregation and dissociation experiments.

Thermogravimetric Analysis: TGA was performed on a Pyris 6 thermogravimetric analyzer (Perkin Elmer Inc.) using Pyris software. Analysis of lyophilized particle samples was performed in pure oxygen atmosphere at a heating rate of $10 \text{ }^\circ\text{C}\cdot\text{min}^{-1}$ from 50 to 800 °C. The mass concentration of iron was calculated from the residual iron oxide.

Atomic Force Microscopy: AFM was measured on mica using a Cypher AFM (Asylum Research) using tapping mode at a scan rate of 1 Hz . Samples were prepared by drop-casting of a particle solution ($\beta = 50 \text{ mg}\cdot\text{L}^{-1}$ in MilliQ water) onto freshly cleaned mica. The sample was dried overnight at room temperature. The AFM images were evaluated using Gwyddion 2.49.

Transmission Electron Microscopy: TEM was performed on a FEI Tecnai G2 Spirit microscope equipped with a Gatan US1000 $2\text{k} \times 2\text{k}$ CCD camera and LaB₆ cathode operated at 120 kV . Images were recorded using freshly glow discharged carbon coated copper grids (CF300-Cu, 300 mesh). For non-stained samples, $5 \mu\text{L}$ nanoparticle solution ($\beta = 50 \text{ mg}\cdot\text{L}^{-1}$ in MilliQ water) was drop-coated on the TEM grid surface and removed with a filter paper after 1 min . For negatively stained samples, $5 \mu\text{L}$ nanoparticle solution ($\beta = 50 \text{ mg}\cdot\text{L}^{-1}$ in MilliQ water) was drop-coated on the TEM grid, removed with a filter paper after 1 min . Next, $5 \mu\text{L}$ uranyl acetate solution (2 wt% in ethanol) were added and removed after 15 s incubation time. All sample-deposited grids were air-dried overnight before measurement. Software ImageJ 1.52h (National Institutes of Health, USA) was used for image evaluation.

For cryogenic TEM (CryoTEM), $5 \mu\text{L}$ of the nanoparticle solution ($50 \text{ g}\cdot\text{L}^{-1}$, in MilliQ water) were applied to freshly glow-discharged carbon grids with a copper 200 mesh (Quantifoil Micro Tools GmbH). Excess fluid was removed by direct blotting (2.5 s) and the grids were individually plunge-frozen in liquid ethane. Grids were cryotransferred in liquid nitrogen using a Gatan cryoholder (model 626 DH) to a Tecnai T12 transmission electron microscope equipped with a field emission electron source and operating at 120 kV accelerating voltage. Images were recorded using a TemCam-F416 (TVIPS, Gauting, Germany). Software ImageJ 1.52h (National Institutes of Health, USA) was used for image evaluation.

Magnetic Response: Images and videos of the magnetic response and particle guidance were recorded using digital single lens reflex cameras Nikon D90 and Nikon D750.

Magnetic data of SPION-CCPMs were collected with the help of a Quantum Design MPMS-XL-7 SQUID magnetometer on powdered sample. ZFC/FC experiments were recorded in a temperature range 4 to 300 K . The sample was cooled to 4 K before applying a field of 100 Oe . The sample was heated to 300 K and subsequently cooled to 4 K with a heating/cooling rate of $1 \text{ K}\cdot\text{min}^{-1}$. The maximum of the ZFC magnetization curve was at $\approx 42 \text{ K}$. Below 44 K a splitting of the ZFC/FC magnetization curve could be observed. Magnetization data were collected at 5 and 300 K with magnetic fields up to $50\,000 \text{ Oe}$.

Fluorescence Correlation Spectroscopy: FCS measurements were performed using a commercial setup, a LSM 880 microscope (Carl Zeiss, Jena, Germany). For excitation of Cy5 an He/Ne-laser (633 nm) was used. The excitation light was focused into the sample by a C-Apochromat $40\times/1.2 \text{ W}$ (Carl, Zeiss, Jena, Germany) water immersion objective. The fluorescence light was collected with the same objective and after passing through a confocal pinhole, directed to a spectral detection unit (Quasar, Carl Zeiss). The detected emission range was in the spectral range of 642 – 696 nm . For calibration of the detection volume Atto Fluor643 was used, as a reference dye with known diffusion coefficient.

The measurements were performed in an eight-well polystyrene-chambered coverglass (Laboratory-Tek, Nalge Nunc International, Penfield, NY, USA). All samples were measured twenty times with a total duration of 3 min . The diffusion of the fluorescent particle through the confocal observation volume caused a time-dependent intensity fluctuation, which could be analyzed by an autocorrelation function:

$$G(\tau) = 1 + \frac{\langle \delta I(t) \cdot \delta I(t + \tau) \rangle}{\langle I(t) \rangle^2} \quad (1)$$

For an ensemble of m different types of freely diffusion fluorescent species, $G(\tau)$ has the following form:^[63]

$$G(\tau) = 1 + \frac{1}{N} \sum_{i=1}^m \frac{f_i}{\left(1 + \frac{\tau}{\tau_{D,i}}\right) \cdot \sqrt{1 + \frac{\tau}{S^2 \cdot \tau_{D,i}}}} \quad (2)$$

N represents the average number of fluorescent species in the observation volume, $\tau_{D,i}$ is the diffusion time of the i -th species, f_i is the fraction of the i -th component and S is the so-called structure factor $S = \frac{z_0}{r_0}$, where z_0 and r_0 represent the axial and radial dimension of the confocal volume, respectively. The diffusion time $\tau_{D,i}$ relates to the diffusion coefficient D_i , through $D_i = \frac{r_0^2}{4 \cdot \tau_{D,i}}$. The hydrodynamic radii R_h can be calculated using

the Stokes–Einstein relation as $R_h = \frac{k_B \cdot T}{6 \cdot \pi \cdot \eta \cdot D}$, where T is the absolute temperature, k_B the Boltzmann constant, and η the viscosity of the solvent.

By fitting the experimental autocorrelation curves with Equation (2), the hydrodynamic radii of the studied nanoparticles were determined. Furthermore, their fluorescence brightness was also determined as $\langle I(t) \rangle / N$. To estimate the average number of Cy5 molecules per particle, the fluorescence brightness of the particles was divided by the fluorescence brightness of the Cy5 molecules.

Multi-Angle Dynamic Light Scattering: For multi-angle DLS cylindrical quartz cuvettes (Hellma, Mühlheim, Germany) were cleaned by dust-free distilled acetone and transferred to a dust free flow box. Light scattering measurements were performed on an ALV spectrometer consisting of a goniometer and an ALV-5004 multiple-tau full-digital correlator (320 channels) which allows measurements over an angular range from 30° to 150°. A He-Ne Laser ($\lambda = 632.8$ nm) was used as light source. The correlation functions of the particles were fitted using a sum of two exponentials. The z-average diffusion coefficient D_z was calculated by extrapolating D_{app} for $q = 0$. By formal application of Stokes law, the inverse z-average hydrodynamic radius is $R_h = \langle R_h^{-1} \rangle_z^{-1}$ was determined. To investigate the aggregation behavior of the particles in human plasma, undiluted citrate plasma was filtered through a Millex GS 0.2 μ m filter. The particle solutions were filtered through 0.45 μ m pore size Millex LCR filters. The following mixtures were prepared from initial particle solutions in PBS ($\beta = 1$ g·L⁻¹): PBS/particle solution 9:1 ($\beta = 0.1$ g·L⁻¹), plasma/PBS 9:1 and plasma/particle solution 9:1 ($\beta = 0.1$ g·L⁻¹). The cuvettes were incubated for 30 min at room temperature before measurement at $T = 20$ °C. Data analysis was performed according to a procedure reported by Rausch et al.^[47] The correlation functions of plasma were fitted with a triexponential decay function, while the particles were fitted using a sum of two exponentials. Mixtures were fitted using a sum of both exponential decay functions with or without an additional aggregate term.

Polymer and Cross-Linker Synthesis: pSar-b-pCys(SO₂Et) block copolymers were prepared by ring-opening NCA polymerization via bifunctional initiator approach, according to Scheme S1, Supporting Information.^[35] Results are summarized in Table S1, Supporting Information. The synthesis of sarcosine NCA and S-ethylsulfonyl-L-cysteine NCA was performed as reported previously.^[34,64]

Synthesis of Poly(sarcosine): Sarcosine NCA (3.00 g, 26.1 mmol, 200 eq.) was transferred into a pre-dried SCHLENK-tube, dissolved in dry DMF (10 mL) and *N*-(*tert*-butoxycarbonyl)-1,2-diaminoethane (20.9 mg, 0.13 mmol, 1.0 eq.) was added via a stock solution in dry DMF. The clear, colorless solution was stirred at 10 °C in the absence of light until the reaction was completed after six days (as monitored by IR spectroscopy). The sarcosine amino terminus was quenched by addition perfluorophenyl 4-azidobutanoate (115 mg, 0.39 mmol, 3.0 eq.) and *N,N*-diisopropylethylamine (133 μ L, 0.78 mmol, 6.0 eq.). The reaction mixture was stirred overnight, followed by addition of acetic anhydride (134 μ L, 1.30 mmol, 10 eq.) and *N,N*-diisopropylethylamine (443 μ L, 2.61 mmol, 20 eq.) to react residual end groups. The slightly yellow solution was stirred for an additional day at room temperature. Precipitation in diethyl ether yielded 1.82 g (97%) of a colorless solid. ¹H NMR (400 MHz, DMSO-*d*₆) δ [ppm] = 4.50–3.76 (m, 2nH, -CH₂-), 3.06–2.76 (m, 3nH, -CH₃), 1.37 (m,

9H, -OC(CH₃)₃). The chain length was determined by HFIP GPC relative to polysarcosine standards.^[62]

The Boc protection group was removed in a mixture of water/trifluoroacetic acid (TFA) (1:1). The polymer (1.82 g) was dissolved in water (32 mL), cooled with an ice bath, followed by addition of TFA (32 mL). After 4 h, the solution was transferred into a dialysis bag (MWCO 3.5 kDa) and dialyzed against MilliQ water, saturated sodium hydrogen carbonate solution, and MilliQ water. The aqueous solution was lyophilized, and the polymer was obtained as a colorless powder (1.65 g, 88%). ¹H NMR (400 MHz, DMSO-*d*₆) δ [ppm] = 4.50–3.76 (m, 2nH, -CH₂-), 3.06–2.76 (m, 3nH, -CH₃).

Synthesis of Poly(sarcosine)_n-Block-Poly(S-ethylsulfonyl-L-cysteine)_m: The poly(sarcosine) macroinitiator (1.58 g, 0.138 mmol, 1.0 eq.) was weighed into a pre-dried SCHLENK-tube and dried by azeotropic distillation with toluene in vacuo. The macroinitiator was dissolved in dry DMF (8.0 mL), cooled to -10 °C, and S-ethylsulfonyl-L-cysteine NCA (1.65 g, 6.90 mmol, 50 eq.) was added as a stock solution in dry DMF. The polymerization was performed at a monomer concentration of $\beta_{NCA} = 110$ g·L⁻¹ and monitored by IR spectroscopy. After 2 days, the conversion was 63% and the reaction was stopped by precipitation in THF. The suspension was centrifuged (4500 rpm, 15 min, 4 °C) and decanted. This procedure was repeated twice concluding with pure diethyl ether. The product was dried in vacuo yielding poly(sarcosine)-block-poly(S-ethylsulfonyl-L-cysteine) (2.30 g, 79%) as a colorless solid. ¹H NMR (400 MHz, DMSO-*d*₆) δ [ppm] = 8.75 (b s, 1mH, NHCO), 4.69 (m, 1mH, α -H_(Cys)), 4.49–3.78 (m, 2nH, -CH₂-_(Sar)), 3.69–3.41 (m, 4mH, -CH₂-S-, -SO₂CH₂-), 3.06–2.61 (m, 3nH, -CH₃(Sar)), 1.30 (t, 3mH, -CH₃(Cys)).

Synthesis of N-(3-azidopropyl)liponamide: The synthesis of N-(3-azidopropyl)-liponamide was performed similar to previous reports.^[35]

Pentafluorophenol lipoate (260 mg, 698 μ mol, 1.0 eq.) was weighed into a pre-dried SCHLENK flask and dissolved in absolute DMF (5.0 mL), before *N,N*-diisopropylethylamine (0.712 mL, 4.19 mmol, 6.0 eq.) and 3-azido-1-propanamine (76.8 mg, 768 μ mol, 1.1 eq.) were added under nitrogen flow. The solution was stirred at room temperature for 16 h. The solvent was removed in vacuo and the reaction mixture was dissolved in dichloromethane (50 mL), washed with water (2 \times 50 mL) and saturated NaHCO₃ solution (2 \times 50 mL). The organic phase was dried over MgSO₄, filtered, and concentrated under reduced pressure. The product purified by column chromatography using dichloromethane/methanol (2%) as eluent and obtained as a yellow liquid (180 mg, 0.625 mmol, 89%). ¹H NMR (400 MHz, CDCl₃) δ [ppm] = 5.63 (s, 1H, -CONH-), 3.57 (dq, ³J = 8.5 Hz, ³J = 6.4 Hz, 1H, dq, -SCH-), 3.36 (m, 4H, -NHCH₂-, -CH₂N₃), 3.14 (m, 2H, -SCH₂-), 2.46 (m, 1H, -SCH₂CH₂-), 2.18 (td, ³J = 7.4 Hz, ³J = 1.2 Hz, 2H, α -CH₂), 1.91 (m, 1H, -SCH₂CH₂-), 1.80 (p, ³J = 6.6 Hz, 2H, -CH₂CH₂N₃), 1.67 (m, 4H, β -CH₂, δ -CH₂), 1.46 (m, 2H, γ -CH₂). ESI-MS $m/z = 289.1$ [M+H]⁺, ([M+H]⁺, (calc.) 289.1 g·mol⁻¹).

Synthesis of SPION-Loaded Core Cross-Linked Polymeric Micelles: Oleic acid-coated SPIONs ($\beta = 5.8$ g L⁻¹, 9.0 mL) dispersed in hexanes were precipitated into 40 mL of ethanol, sonicated for 15 min and sedimented (4500 rpm, 15 min, 20 °C). The pellet was resuspended in 5.0 mL of chloroform, sonicated for 30 min, precipitated in 45 mL of ethanol, and sedimented (4500 rpm, 15 min, 20 °C) to remove excess oleic acid. SPIONs were resuspended in 20 mL of chloroform and a polymer solution in DMSO/CHCl₃ (1:2) ($\beta = 5.0$ g L⁻¹, 10 mL) was added dropwise. The resulting clear brown solution was placed in a dialysis bag (MWCO 3.5 kDa) and dialyzed against CHCl₃, followed by dialysis against DMSO. The solution was diluted with DMSO by factor 2 and dialyzed against MilliQ water to obtain SPION-loaded polymeric micelles. The obtained micelles were filtered through a PVDF 0.45 μ m filter and concentrated to a total volume of 8.0 mL by spin filtration (Amicon Ultra-15, MWCO 3.0 kDa, 4500 rpm, 20 °C). For core cross-linking, *D,L*-lipoic acid (8.0 mg, 39.1 μ mol, 0.5 eq. per pCys(SO₂Et) repeating unit) was dissolved in ethanol (5.0 g L⁻¹) and treated with tris(2-carboxyethyl)phosphine hydrochloride (11.2 mg, 39.1 μ mol, 50 g L⁻¹ in MilliQ water) for 18 h yielding dihydro lipoic acid. The cross-linker solution was added to the micelle solution and the reaction mixture was placed on a benchtop shaker for 24 h. Subsequently, excess cross-linker and residual oleic acid were removed by dialysis (MWCO 3.5 kDa) against DMSO/MilliQ water mixtures (1:1) followed

by dialysis against MilliQ water yielding a clear light brown solution. For dye conjugation, the SPION-CCPM solution was adjusted to pH 7.4 using 1 M sodium hydrogen carbonate solution, Cy5-NHS ester (540 μg , 0.3 eq. per polymer, 25 g L^{-1} in DMSO) was added, and the solution was stirred at room temperature for 72 h. Upon addition of the blue dye solution, the particle solution turned dark green immediately. The excess dye was removed by repetitive extraction with dichloromethane, followed by dialysis against ethanol/MilliQ water mixtures (1:1) and MilliQ water (MWCO 6–8 kDa). To remove the free polymer, Cy5-labelled SPION-CCPMs (SPION-CCPM^{Cy5}) were purified by repetitive spin filtration (Amicon Ultra-15, MWCO 100 kDa, 3000 rpm, 20 °C), and finally concentrated to a total volume of 8.5 mL, yielding 23 mg of SPION-CCPM^{Cy5} (overall yield 23%).

Synthesis of Core Cross-Linked Polymeric Micelles (Control-Particles): The preparation of CCPMs was performed as described previously.^[35,37]

Poly(sarcosine)-block-poly(S-ethylsulfonyl-L-cysteine) (pSar₂₂₅-b-pCys(SO₂Et)₃₁) was dissolved in DMSO equipped with 1 M thiourea at a concentration of 7.5 g L^{-1} for 1 h. Next, 20 vol% of 1 M acetate buffer (pH 4.75) with 10 mM thiourea were added to adjust the concentration to 6.6 g L^{-1} . The solution was left to equilibrate at room temperature for 5 h, followed by dialysis against 1 M acetate buffer (pH 4.75) with 10 mM thiourea. The solution was filtered (GHP 450) and concentrated to 6.6 g L^{-1} by spin filtration (Amicon Ultra, MWCO 3 kDa), yielding the micelle solution. For cross-linking, in a separate flask, N-3-azidopropyl liponamide was dissolved in ethanol at a concentration of $\beta = 10 \text{ g L}^{-1}$ and one equivalent of an aqueous solution of TCEP-HCl (50 g L^{-1}) was added per disulfide. After 18 h, the cross-linker solution was added to the micelle solution at equimolar amounts of thiols per cysteines. The reaction mixture was allowed to stand at room temperature for 48 h. To remove residual cross-linker and free polymer, the solution was dialyzed against DMSO and MilliQ water (MWCO 6–8 kDa), followed by repetitive spin filtration (Amicon Ultra, MWCO 100 kDa). For labeling, the pH was adjusted to 7.4 (1 M NaHCO₃ solution) and 0.3 equivalents of Cyanine 5-NHS-ester stock solution in DMSO (25 g L^{-1}) were added per polymer end-group. After 72 h, excess dye was removed by repetitive spin filtration (Amicon Ultra, 100 kDa) using ethanol/water mixtures and the final particle solution (in MilliQ water) was stored at 4 °C. The absence of free polymer and free dye was verified by GPC in hexafluoro isopropanol.

Isolation of Bone Marrow-Derived Macrophages: The procedure conducted follows previously established protocol.^[65] Briefly, bone marrow cells were flushed from the tibia and femurs of C57BL/6N wild-type mice (8–10 weeks of age) using ice cold Hanks' Balanced Salt Solution (HBSS), filtered through a 70 μm filter cell strainer and plated at a density of $3.5 \times 10^5 \text{ cells mL}^{-1}$. Cells were differentiated for one-week using RPMI medium supplemented with 10 ng mL^{-1} M-CSF (M9170, Sigma Aldrich), 10% fetal bovine serum (FBS) and 1% penicillin/streptomycin (Gibco). For each independent experiment, BMDMs were prepared from three different mice.

Cell Lines: LLC cells were regularly tested for mycoplasma contamination and authenticated by visual observations of cell morphology. Cells were cultured in Roswell Park Memorial Institute Medium (RPMI, Life Technologies) containing 10% FBS and 1% penicillin/streptomycin.

Hepatocyte Isolation: Hepatocytes from C57BL/6N wild-type mice (8–10 weeks of age) were prepared following a standard two-step perfusion method.^[66–68] Briefly, liver perfusion (Life Technologies #17701038) and liver digest medium (Life Technologies #17703-034) were pumped into the liver through the cava vein with a 5 mL min^{-1} flux rate. The liver capsule was mechanically disrupted in hepatocyte wash medium (Life Technologies #17704-024). The cell suspension obtained was passed through 100 μm filter and centrifuged for 5 min at 50 G and 4 °C. The pellet of hepatocytes was resuspended in William's E medium (Life Technologies #32551-020) supplemented with 4% FBS and $2.50 \times 10^5 \text{ cells mL}^{-1}$ were plated on 13 mm collagen-coated (Life Technologies #A1048301) glass cover slips.

Mice: 10 female C57BL/6 mice, aged 6–8 weeks, were housed in specific pathogen-free conditions under constant light-dark cycle and maintained on a standard mouse diet. Experimentation was performed at the DKFZ animal facilities, in accordance with institutional guidelines, and

were approved by the Regierungspräsidium Karlsruhe, Germany, under permit number G214/19. Mice were anaesthetized by intraperitoneal injection of 100 $\mu\text{g g}^{-1}$ ketamine and 14 $\mu\text{g g}^{-1}$ xylazine and intratracheally instilled with SPION-CCPM (10 mg kg^{-1} of iron to body weight) or PBS in a final volume of 50 μL .

Immunofluorescence: BMDMs were plated on 13 mm collagen-coated (Life Technologies #A1048301) glass cover slips in a density of $1.0 \times 10^5 \text{ cells per slip}$. After treatment, cells were washed three times with PBS and fixed with 4% paraformaldehyde for 15 min at room temperature. Cells were then washed three times with PBS and blocked with 2.5% milk in PBS-T (0.1% Tween) solution for 30 min on an orbital shaker. Slips were then washed three times with 0.1% PBS-T and incubated with primary antibody Iba1 (NB100-1028SS, Bio Techne) overnight at 4 °C or 1 h at room temperature. After washing with PBS-T, samples were incubated with secondary antibody (A-11057, Donkey anti-Goat IgG (H+L) Cross-adsorbed Secondary Antibody Alexa Fluor 568, Life Technologies) for 1 h at room temperature. Slips were then washed with PBS and mounted using Prolong Gold Antifade Mountant with DAPI (P36931, Life Technologies). Samples were acquired at the University of Heidelberg Nikon Imaging Centre using a Ni-E confocal microscope. Images were analyzed using Fiji (National Institute for Health) using a written macro for intracellular quantification of the Cy5+ signal. Images were compiled into figures using Adobe Photoshop and Illustrator.

Flow Cytometry: Mouse lungs were resected and washed in PBS. Single cell suspensions (200 μL) were generated by applying chemical and mechanical digestion using the Miltenyi Lung Dissociation Kit and pelleted by centrifugation for 5 min at 300 G. Cells were then washed with FACS buffer (1% FBS, 2.5 mM 1 M HEPES, 1 mM EDTA) prior to antibody staining. Cells were stained with anti-mouse CD45-PERCPCy5.5 (BD Biosciences), LY6G-FITC (BioLegend, California, USA), LY6C-PEDAZZLE (BD Biosciences), F4/80-BV605 (BioLegend, California, USA), CD11C-PE (BioLegend, California, USA), SIGLECF-APCCY7 (BD Biosciences), CD11B-PERCP (BD Biosciences), CD64-BV711 (BioLegend, California, USA), CD80-BV650 (BioLegend, California, USA), CD71-BV510 (BioLegend, California, USA), MERTK-BV421 (BD Biosciences), and the viability stain DAPI (BioLegend, California, USA). Samples were acquired using Cytotek Aurora flow cytometer at the EMBL Flow Cytometry Core Facility and analysis was performed using the FlowJo Software (Tree Star Inc.).

BMDMs were incubated with Fc γ receptor blocking solution and stained with anti-mouse CD206-FITC, CD86-PE, MHC II-PeCy5 (BioLegend, California, USA), CD301-PerCPCy5.5, CD38-FITC (BD Biosciences), and the viability staining solution 7AAD (420404, Biozol; see Table S3, Supporting Information). Data were acquired using a FACS Fortessa (BD, Biosciences) or Cytotek Aurora flow cytometer at the EMBL Flow Cytometry Core Facility and analysis was performed using the FlowJo Software (Tree Star Inc.). The expression of surface markers in mouse lung cells and BMDM was calculated by subtracting the geometric median fluorescence intensity (MFI) of cells stained with the isotype-matched antibody from the MFI of those stained with the specific antibody and was shown as fold-change compared to the non-treated (NT) control.

Tissue Non-Heme Iron Measurement: Lungs of mice were measured for non-heme iron content using the bathophenanthroline method and calculated against dry weight of tissue.^[69]

Cytotoxicity: BMDM viability was quantified using CytoTox96 kit from Promega. Cells were plated in a black side/black bottom 96 well plate at a concentration of 10 000 cells in 100 μL per well 24 h before start of the experiment. To measure LDH release into the supernatant, plate was centrifuged at 500 G for 10 min to sediment cells and 100 μL was transferred to a new 96 well plate. 50 μL of substrate was added to 50 μL of supernatant and incubated for 30 min at room temperature in the dark. After 30 min, 20 μL stop solution was added to each well and the 490 nm signal was measured in a spectrofluorimeter (SpectraMax, Molecular Devices). Viability was calculated by subtracting the media blank from experimental values and normalized to the NT condition. To measure redox capacity, after incubation times with conditions, 10 μL of Celltiter Blue was added to each well and plate was incubated at 37 °C for 4 h. Absorbance was then

measured at 520 nm and all values were subtracted from the media blank control and normalized to the NT condition.

RNA Extraction, Reverse Transcription, and Quantitative Real-Time Polymerase Chain Reaction Analysis: RNA was extracted from lung tissue using Trizol (Life Technologies). RNA was extracted from BMDMs using the RNeasy Mini Kit (74134, Qiagen). 0.5 to 1 µg of total RNA was reverse transcribed by using RevertAid H Minus Reverse Transcriptase (FERMEP0452, Thermo Scientific), random primers (48190-011, Invitrogen), and dNTPs (R0193, ThermoScientific). SYBR green qRT-PCR was performed on a Step One Plus Real Time PCR System (Applied Biosystems, California, USA). Primers and probes were designed using the ProbeFinder software (www.roche-applied-science.com; see Table S4, Supporting Information). Differences in relative quantity were shown as fold-change compared to the control condition (untreated cells, NT).

Measurement of Intracellular ROS Accumulation: Accumulation of ROS in BMDM cells was assessed by using the oxidant-sensitive fluorescent dye CELLROX Green and CELLROX Orange (Life Technologies). Upon cellular uptake, the non-fluorescent CELLROX probe undergoes deacetylation by intracellular esterases producing a highly green fluorescent signal following oxidation by intracellular ROS. BMDMs were maintained untreated or were treated for 4 or 18 h with 20 µM SPION-CCPMs, CCPMs, 100 ng mL⁻¹ LPS or interferon-γ, 20 µM FAC, or 20 µM heme. The amount of SPION-CCPMs added to cells was calculated to 20 µM iron from within the core. Then the amount of CCPMs added to cells was calculated to match the mass of CCPMs contained within added SPION-CCPMs. 2.5 mm of CELLROX Green or Orange was added to cells and incubated for 30 min at 37 °C under 5% CO₂ atmosphere. Cells were washed twice with HBSS and fluorescence intensity was measured using FACS. Fluorescence intensity was represented as fold change compared to the NT condition.

Protein Extraction and Western Blotting: Protein lysates were obtained by homogenizing cells in RIPA buffer supplemented with protease inhibitors (Roche Diagnostics). Protein concentration was determined using the DC Protein Assay Kit II system (5000112, Bio-Rad, München, Germany). 50 µg of total protein extracts were separated by 12% SDS-PAGE and analyzed by Western blotting using antibodies against HO-1 (Stressgen, Victoria, Canada) or TfR1 (136800, Invitrogen/Life Tech). β-actin (A1978-200UL, Sigma Aldrich) was used as a loading control. Densitometric analysis was reported in Arbitrary Unit (AU), as ratio to the untreated (NT) sample (AU = 1). Western blot images were quantitatively acquired with the Vilber Lourmat Fusion-FX Chemiluminescence system (Eberhardzell).

Perls' Prussian Blue Staining: 3.5 × 10⁵ BMDMs were plated on a 13 mm (Life Technologies #A1048301) glass slips. After incubation or treatment, cells were washed three times with PBS and fixed with 4% paraformaldehyde at room temperature for 10 min. Cells were then washed three times with PBS and stained with Accustain Iron Stain No. HT20 (Sigma Aldrich) following manufacturer's instructions and counterstained with Fast Red (Sigma Aldrich). Samples were mounted using the water-soluble mounting agent VectaMount (H5501, Biozol). Images were digitally acquired with a Nikon Ni-E microscope, using the Nikon NIS-Elements Viewer software and assembled into figures using Adobe Photoshop and Illustrator software packages.

Buffy Coat Preparation: Human monocytes were isolated from commercially available buffy coats (DRK-Blutspendedienst Baden-Württemberg-Hessen, Frankfurt, Germany) using Ficoll-Hypaque gradients (LSM-1077; PAA Laboratories). Monocytes were differentiated into primary human macrophages with RPMI 1640 containing 5% AB-positive human serum (DRK-Blutspendedienst) for 7 days and achieved ≈80% confluence. 24 h prior to stimulation, cells were serum starved. Cells were then prepared to analyze cell surface expression of proteins by FACS measurement (antibodies in Table S3, Supporting Information) or differential mRNA expression by qPCR (primers in Table S5, Supporting Information).

Statistical Analysis: Data were shown as mean ± SEM. Statistical analyses were performed using Prims v10 (GraphPad Software, La Jolla, CA). One-way ANOVA was used and *p*-values < 0.05 (*), < 0.01 (**), < 0.001 (***), and < 0.0001 (****) were indicated.

Supporting Information

Supporting Information is available from the Wiley Online Library or from the author.

Acknowledgements

T.A.B. and N.K.H. contributed equally to this work and are both appointed as first authors. T.A.B., S.S., K.K., and M.B. acknowledge funding by the SFB1066-2. T.A.B. would like to thank the HaVo Stiftung and the Max Planck Graduate Center for financial support. N.K.H. would like to acknowledge Dr. Sandro Altamura for scientific discussions and assistance; Dr. Thomas Schwarzl for statistical consultation; and Richard Sparla for experimental assistance. The authors acknowledge Christine Rosenauer (MPIP) for assistance, and Dr. Frank Depoix for support on the TEM. The authors thank the personnel of the animal facility of the Heidelberg University for the mouse housing and care. M.U.M. acknowledges funding from the DFG (SFB1036, SFB1118) from the Federal Ministry of Education and Research (NephrESA Nr 031L0191C) and from the Ministry of Science, Research and the Arts (MWK) Baden-Württemberg (DZL TLRC-H). N.K.H. would like to thank the EMBL Flow Cytometry Core Facility, especially Dr. Malte Paulsen and Dr. Diana Ordonez, for training, discussions, and technical assistance. N.K.H. and M.U.M. would like to thank the Nikon Imaging Center at the University of Heidelberg for use of their facility.

Conflict of Interest

T.A.B., N.K.H., M.U.M., M.W.H., and M.B. have submitted the patent application "SPION-CCPM; Nanoparticles Comprising Iron Oxide Particles Embedded in Polymeric Micelles" EP 20 210 176.2.

Data Availability Statement

The data that support the findings of this study are available from the corresponding author upon reasonable request.

Keywords

cross-linking, iron metabolism, macrophage polarization, polymeric micelle, polypeptide, superparamagnetic iron oxide nanoparticles

Received: April 18, 2021
Published online: June 16, 2021

- [1] M. Costa da Silva, M. O. Breckwoldt, F. Vinchi, M. P. Correia, A. Stojanovic, C. M. Thielmann, M. Meister, T. Muley, A. Warth, M. Platten, M. W. Hentze, A. Cerwenka, M. U. Muckenthaler, *Front. Immunol.* **2017**, *8*, 1479.
- [2] J. A. Ardura, G. Rackov, E. Izquierdo, V. Alonso, A. R. Gortazar, M. M. Escribese, *Front. Pharmacol.* **2019**, *10*, 1255.
- [3] G. Chinetti-Gbaguidi, B. Staels, *Curr. Opin. Lipidol.* **2011**, *22*, 365.
- [4] N. K. Tangudu, B. Alan, F. Vinchi, K. Wörle, D. Lai, S. Vettorazzi, K. Leopold, M. Vujčić Spasić, *Antioxid. Redox Signaling* **2018**, *29*, 484.
- [5] B. Ruffell, L. M. Coussens, *Cancer Cell* **2015**, *27*, 462.
- [6] P. J. Murray, *Annu. Rev. Physiol.* **2017**, *79*, 541.
- [7] G. Cairo, S. Recalcati, A. Mantovani, M. Locati, *Trends Immunol.* **2011**, *32*, 241.
- [8] Y. Bao, J. A. Sherwood, Z. Sun, *J. Mater. Chem. C* **2018**, *6*, 1280.
- [9] R. E. Mebius, G. Kraal, *Nat. Rev. Immunol.* **2005**, *5*, 606.

- [10] A. Sica, A. Mantovani, *J. Clin. Invest.* **2012**, 122, 787.
- [11] C. E. Lewis, J. W. Pollard, *Cancer Res.* **2006**, 66, 605.
- [12] J. L. Guerriero, *Trends Mol. Med.* **2018**, 24, 472.
- [13] V. Davra, S. Kimani, D. Calianese, R. Birge, *Cancers* **2016**, 8, 107.
- [14] S. Recalcati, M. Locati, A. Marini, P. Santambrogio, F. Zaninotto, M. De Pizzol, L. Zammataro, D. Girelli, G. Cairo, *Eur. J. Immunol.* **2010**, 40, 824.
- [15] N. Sukhbaatar, T. Weichhart, *Pharmaceuticals* **2018**, 11, 137.
- [16] M. W. Hentze, M. U. Muckenthaler, B. Galy, C. Camaschella, *Cell* **2010**, 142, 24.
- [17] M. U. Muckenthaler, S. Rivella, M. W. Hentze, B. Galy, *Cell* **2017**, 168, 344.
- [18] F. Vinchi, M. Costa da Silva, G. Ingoglia, S. Petrillo, N. Brinkman, A. Zuercher, A. Cerwenka, E. Tolosano, M. U. Muckenthaler, *Blood* **2016**, 127, 473.
- [19] S. Zanganeh, G. Hutter, R. Spitler, O. Lenkov, M. Mahmoudi, A. Shaw, J. S. Pajarinen, H. Nejadnik, S. Goodman, M. Moseley, L. M. Coussens, H. E. Daldrop-Link, *Nat. Nanotechnol.* **2016**, 11, 986.
- [20] G. Wang, J. Zhao, M. Zhang, Q. Wang, B. Chen, Y. Hou, K. Lu, *Int. J. Nanomed.* **2019**, 14, 4503.
- [21] J. Zhao, Z. Zhang, Y. Xue, G. Wang, Y. Cheng, Y. Pan, S. Zhao, Y. Hou, *Theranostics* **2018**, 8, 6307.
- [22] R. Jin, L. Liu, W. Zhu, D. Li, L. Yang, J. Duan, Z. Cai, Y. Nie, Y. Zhang, Q. Gong, B. Song, L. Wen, J. M. Anderson, H. Ai, *Biomaterials* **2019**, 203, 23.
- [23] V. Trujillo-Alonso, E. C. Pratt, H. Zong, A. Lara-Martinez, C. Kaittanis, M. O. Rabie, V. Longo, M. W. Becker, G. J. Roboz, J. Grimm, M. L. Guzman, *Nat. Nanotechnol.* **2019**, 14, 616.
- [24] K. El-Boubbou, *Nanomedicine* **2018**, 13, 953.
- [25] V. S. Balakrishnan, M. Rao, A. T. Kausz, L. Brenner, B. J. G. Pereira, T. B. Frigo, J. M. Lewis, *Eur. J. Clin. Invest.* **2009**, 39, 489.
- [26] European Medicines Agency, Rienso: Withdrawal of the Marketing Authorization in the European Union, **2015**.
- [27] S. M. Dadfar, K. Roemhild, N. I. Drude, S. von Stillfried, R. Knüchel, F. Kiessling, T. Lammers, *Adv. Drug Delivery Rev.* **2019**, 138, 302.
- [28] R. Weissleder, D. Stark, B. Engelstad, B. Bacon, C. Compton, D. White, P. Jacobs, J. Lewis, *Am. J. Roentgenol.* **1989**, 152, 167.
- [29] M. Lu, M. H. Cohen, D. Rieves, R. Pazdur, *Am. J. Hematol.* **2010**, 85, 315.
- [30] G. B. Toth, C. G. Varallyay, A. Horvath, M. R. Bashir, P. L. Choyke, H. E. Daldrop-Link, E. Dosa, J. P. Finn, S. Gahramanov, M. Harisinghani, I. Maccougall, A. Neuwelt, S. S. Vasanawala, P. Ambady, R. Barajas, J. S. Cetas, J. Ciporen, T. J. DeLoughery, N. D. Doolittle, R. Fu, J. Grinstead, A. R. Guimaraes, B. E. Hamilton, X. Li, H. McConnell, L. L. Muldoon, G. Nesbit, J. P. Netto, D. Petterson, W. D. Rooney, D. Schwartz, L. Szidonya, E. A. Neuwelt, *Kidney Int.* **2017**, 92, 47.
- [31] A. Birke, J. Ling, M. Barz, *Prog. Polym. Sci.* **2018**, 81, 163.
- [32] K. Klinker, M. Barz, *Macromol. Rapid Commun.* **2015**, 36, 1943.
- [33] C. S. Sevier, C. A. Kaiser, *Nat. Rev. Mol. Cell Biol.* **2002**, 3, 836.
- [34] A. Birke, D. Huesmann, A. Kelsch, M. Weibäcker, J. Xie, M. Bros, T. Bopp, C. Becker, K. Landfester, M. Barz, *Biomacromolecules* **2014**, 15, 548.
- [35] K. Klinker, O. Schäfer, D. Huesmann, T. Bauer, L. Capelôa, L. Braun, N. Stergiou, M. Schinnerer, A. Dirisala, K. Miyata, K. Osada, H. Cabral, K. Kataoka, M. Barz, *Angew. Chem., Int. Ed.* **2017**, 56, 9608.
- [36] M. Talelli, M. Barz, C. J. F. F. Rijcken, F. Kiessling, W. E. Hennink, T. Lammers, *Nano Today* **2015**, 10, 93.
- [37] N. K. Dal, A. Kocer, J. Wohlmann, S. Van Herck, T. A. Bauer, J. Resseguier, S. Bagherifam, H. Hyldmo, M. Barz, B. G. De Geest, F. Fenaroli, *Small* **2020**, 16, 1906719.
- [38] T. Ojha, Q. Hu, C. Colombo, J. Wit, M. van Geijn, M. J. van Steenberg, M. Bagheri, H. Königs-Werner, E. M. Buhl, R. Bansal, Y. Shi, W. E. Hennink, G. Storm, C. J. F. Rijcken, T. Lammers, *Biotechnol. J.* **2021**, 16, 2000212.
- [39] B.-S. Kim, J.-M. Qiu, J.-P. Wang, T. A. Taton, *Nano Lett.* **2005**, 5, 1987.
- [40] M. Talelli, C. J. F. Rijcken, T. Lammers, P. R. Seevinck, G. Storm, C. F. Van Nostrum, W. E. Hennink, *Langmuir* **2009**, 25, 2060.
- [41] C. Schmidtke, R. Eggers, R. Zierold, A. Feld, H. Kloust, C. Wolter, J. Ostermann, J. P. Merkl, T. Schotten, K. Nielsch, H. Weller, *Langmuir* **2014**, 30, 11190.
- [42] E. Amstad, S. Zurcher, A. Mashaghi, J. Y. Wong, M. Textor, E. Reimhult, *Small* **2009**, 5, 1334.
- [43] E. Karaoğlu, A. Baykal, H. Erdemi, L. Alpsoy, H. Sozeri, *J. Alloys Compd.* **2011**, 509, 9218.
- [44] A. Demortière, P. Panissod, B. P. Pichon, G. Pourroy, D. Guillon, B. Donnio, S. Bégin-Colin, *Nanoscale* **2011**, 3, 225.
- [45] O. Baun, P. Blümler, *J. Magn. Magn. Mater.* **2017**, 439, 294.
- [46] a) R. Kawasaki, Y. Sasaki, K. Katagiri, S. Mukai, S. Sawada, K. Akiyoshi, *Angew. Chem.* **2016**, 128, 11549. b) R. Kawasaki, Y. Sasaki, K. Katagiri, S. Mukai, S. Sawada, K. Akiyoshi, *Angew. Chem., Int. Ed.* **2016**, 55, 11377.
- [47] K. Rausch, A. Reuter, K. Fischer, M. Schmidt, *Biomacromolecules* **2010**, 11, 2836.
- [48] K. Koynov, H. J. Butt, *Curr. Opin. Colloid Interface Sci.* **2012**, 17, 377.
- [49] M. Mahmoudi, S. Sant, B. Wang, S. Laurent, T. Sen, *Adv. Drug Delivery Rev.* **2011**, 63, 24.
- [50] F. Michelet, R. Gueguen, P. Leroy, M. Wellman, A. Nicolas, G. Siest, *Clin. Chem.* **1995**, 41, 1509.
- [51] S. M. U. Ahmed, L. Luo, A. Namani, X. J. Wang, X. Tang, *Biochim. Biophys. Acta, Mol. Basis Dis.* **2017**, 1863, 585.
- [52] N. Shenoy, M. Stenson, J. Lawson, J. Abeykoon, M. Patnaik, X. Wu, T. Witzig, *Lab. Invest.* **2017**, 97, 494.
- [53] C. M. Thielmann, M. Costa da Silva, T. Muley, M. Meister, E. Herpel, M. U. Muckenthaler, *Sci. Rep.* **2019**, 9, 11326.
- [54] M. Ponzoni, F. Pastorino, D. Di Paolo, P. Perri, C. Brignole, *Int. J. Mol. Sci.* **2018**, 19, 1953.
- [55] W.-H. Lee, C.-Y. Loo, D. Traini, P. M. Young, *Expert Opin. Drug Delivery* **2015**, 12, 1009.
- [56] *Nanocarriers: Drug Delivery System* (Ed: N. Shah), Springer, Singapore **2021**, p. 3.
- [57] A. Chakraborty, S. Royce, C. Selomulya, M. Plebanski, *Int. J. Mol. Sci.* **2020**, 21, 1613.
- [58] T. Shi, L. Denney, H. An, L. Ho, Y. Zheng, *J. Leukocyte Biol.* **2020**.
- [59] D. Bedoret, H. Wallemacq, T. Marichal, C. Desmet, F. Quesada Calvo, E. Henry, R. Closset, B. Dewals, C. Thielen, P. Gustin, L. de Leval, N. van Rooijen, A. Le Moine, A. Vanderplasschen, D. Cataldo, P. V. Drion, M. Moser, P. Lekeux, F. Bureau, *J. Clin. Invest.* **2009**, 119, 3723.
- [60] B. Cai, C. Kasikara, A. C. Doran, R. Ramakrishnan, R. B. Birge, I. Tabas, *Sci. Signaling* **2018**, 11, eaar3721.
- [61] T. R. Ulich, L. R. Watson, S. Yin, K. Guo, P. Wang, H. Thang, J. Del Castillo, *Am. J. Pathol.* **1991**, 138, 1485.
- [62] B. Weber, A. Birke, K. Fischer, M. Schmidt, M. Barz, *Macromolecules* **2018**, 51, 2653.
- [63] R. Rigler, E. S. Elson, *Fluorescence Correlation Spectroscopy: Theory and Applications*, Springer, Berlin **2012**.
- [64] O. Schäfer, D. Huesmann, C. Muhl, M. Barz, *Chem. - Eur. J.* **2016**, 22, 18085.
- [65] C. Guida, S. Altamura, F. A. Klein, B. Galy, M. Boutros, A. J. Ulmer, M. W. Hentze, M. U. Muckenthaler, *Blood* **2015**, 125, 2265.
- [66] J. E. Klaunig, P. J. Goldblatt, D. E. Hinton, M. M. Lipsky, B. F. Trump, *In Vitro* **1981**, 17, 913.
- [67] J. E. Klaunig, P. J. Goldblatt, D. E. Hinton, M. M. Lipsky, B. F. Trump, *In Vitro* **1981**, 17, 926.
- [68] M. Severgnini, J. Sherman, A. Sehgal, N. K. Jayaprakash, J. Aubin, G. Wang, L. Zhang, C. G. Peng, K. Yucius, J. Butler, K. Fitzgerald, *Cytotechnology* **2012**, 64, 187.
- [69] J. D. Torrance, T. H. Bothwell, *S. Afr. J. Med. Sci.* **1968**, 33, 9.